The Astrophysical Journal, 865:122 (17pp), 2018 October 1 https://doi.org/10.3847/1538-4357/aada7d
© 2018. The American Astronomical Society. All rights reserved.

Strong Lensing Modeling in Galaxy Clusters as a Promising Method to Test Cosmography. I. Parametric Dark Energy Models

Juan Magaña[1], Ana Acebrón[2,3], Verónica Motta[1], Tomás Verdugo[4], Eric Jullo[2], and Marceau Limousin[2]
[1] Instituto de Física y Astronomía, Facultad de Ciencias, Universidad de Valparaíso, Avda. Gran Bretaña 1111, Valparaíso, Chile; juan.magana@uv.cl
[2] Aix Marseille Univ, CNRS, CNES, LAM, Marseille, France
[3] Physics Department, Ben-Gurion University of the Negev, P.O. Box 653, Be'er-Sheva 8410501, Israel
[4] Instituto de Astronomía, Universidad Nacional Autónoma de México, Apartado postal 106, C.P. 22800, Ensenada, B.C., México
Received 2017 October 31; revised 2018 August 13; accepted 2018 August 13; published 2018 September 28

Abstract

In this paper we probe five cosmological models for which the dark energy equation of state parameter, $w(z)$, is parameterized as a function of redshift using strong lensing data in the galaxy cluster Abell 1689. We constrain the parameters of the $w(z)$ functions by reconstructing the lens model under each one of these cosmologies with strong lensing measurements from two galaxy clusters, Abell 1689 and a mock cluster, Ares, from the Hubble Frontier Fields Comparison Challenge, to validate our methodology. To quantify how the cosmological constraints are biased due to systematic effects in the strong lensing modeling, we carry out three runs considering the following uncertainties for the multiple image positions: $0\farcs25$, $0\farcs5$, and $1\farcs0$. With Ares, we find that larger errors decrease the systematic bias on the estimated cosmological parameters. With real data, our strong-lensing constraints on $w(z)$ are consistent with those derived from other cosmological probes. We confirm that strong lensing cosmography with galaxy clusters is a promising method to constrain $w(z)$ parameterizations. A better understanding of galaxy clusters and their environment is needed, however, to improve the SL modeling and hence to estimate stringent cosmological parameters in alternative cosmologies.

Key words: cosmological parameters – dark energy – gravitational lensing: strong

1. Introduction

Current cosmological observations provide strong evidence that the expansion of the universe is accelerating (Riess et al. 1998; Perlmutter et al. 1999; Planck Collaboration et al. 2016b). The source of this cosmic acceleration is a big puzzle in modern cosmology and two approaches have been adopted to explain it: either to postulate the existence of a dark energy component or to modify the gravity laws (Joyce et al. 2016). Among the former, the cosmological constant, which is commonly associated with the quantum vacuum energy, has been established as the preferred candidate to investigate the nature of dark energy using several cosmological measurements (e.g., Planck Collaboration et al. 2016a). By definition, the equation of state (EoS, hereafter) parameter of the cosmological constant is $w=-1$. Nonetheless, when a general constant EoS is considered, the data constrain $w=-1.019^{+0.075}_{-0.080}$ (Planck Collaboration et al. 2016b, see also Neveu et al. 2017), which is consistent with the cosmological constant. In spite of this consistency, the theoretical expected value of the vacuum energy differs in many orders of magnitude from the observed one. In addition, the coincidence problem, i.e., the similitude seen at the current time between the dark matter energy density and that of DE, remains unsolved (Zeldovich 1968; Weinberg 1989). Several dark energy (DE, hereafter) models such as, for instance, dynamical dark energy or interacting dark energy (IDE; Copeland et al. 2006; Li et al. 2011), are also in agreement with the data and they can satisfactorily describe the late-time acceleration of the universe in a similar way as the cosmological constant does (Salvatelli et al. 2014; Ferreira et al. 2017; Zhao et al. 2017). Therefore, to distinguish which cosmological model is more suitable to investigating the nature of dark energy, we need to put tight constraints on their parameters. A standard way to estimate these parameters is to perform a Bayesian analysis using classic cosmological probes, i.e., to fit the distance modulus of type Ia distant supernovae (SNe Ia), Hubble parameter measurements, baryon acoustic oscillation (BAO) signals, and the acoustic peaks of the cosmic microwave background (CMB) radiation (Davis 2014; Mortonson et al. 2014). Although these tests are widely used to constrain cosmological models, they could yield to biased estimations because either the data or the test fitting formulas are derived assuming an underlying standard cosmology ΛCDM (i.e., the cosmological constant as dark energy plus cold dark matter). Thus, it is essential to construct methods to estimate the parameters of alternative cosmologies without assuming any fiducial cosmology. One novel technique is to use strong lensing measurements in galaxy clusters.

Strong gravitational lensing (SL, hereafter) offers a unique and independent opportunity to constrain dark energy features without prior assumptions on the fiducial cosmology. Link & Pierce (1998) introduced a new approach by leveraging the cosmological sensitivity of the angular size-redshift relation when multiples imaged systems (over a broad range of redshift) are produced by strong lensing clusters. This technique was later on extended to more complex simulated clusters by Golse et al. (2002) and to real clusters such as Abell 2218 (see Soucail et al. 2004), showing that SL cosmography is a promising geometrical cosmological test. Jullo et al. (2010) used an improved technique that simultaneously reconstructed the mass distribution of Abell 1689 (A1689, hereafter), adopting a parametric lens modeling, and constrained the parameters of a wCDM cosmology. For the first time, the authors obtained competitive constraints on the EoS parameter and found that, by combining their results with other probes, they improved the

DE EoS estimation by ∼30%. Following the same method, Caminha et al. (2016) recently used the SL measurements in Abell S1063 with the pre-*Frontier Fields* data to constrain cosmological parameters for three different ΛCDM models. They pointed out the importance of estimating the parameters using multiply lensed sources with a wide range of redshifts. The authors also showed that the lack of spectroscopic measurements or the use of inaccurate photometric redshifts leads to a biased estimation of the cosmological parameters. Magaña et al. (2015) exploited this technique too, but using alternative cosmologies. They used A1689 strong lensing measurements to constrain four dark energy models: Chevallier–Polarski–Linder (CPL), IDE, Ricci Holographic Dark Energy (RHDE), and Modified Polytropic Cardassian. They found that the SL method provides CPL constraints in good agreement with those obtained with the SNe Ia, BAO, and CMB data. In addition, the IDE and RHDE constraints derived from SL are similar to those estimated with other tests. Nevertheless, the IDE constraints are consistent with the complementary bounds only if an increase in the image-position error (five times the one previously used by Jullo et al. 2010) is considered in the lens modeling. They confirmed that, to avoid misleading DE bounds, it is important to consider larger positional uncertainties for the multiple images—which could be associated with systematic errors.

Indeed, SL has various known sources of systematic errors. D'Aloisio & Natarajan (2011), using simulations of cluster lenses, showed that the observational errors (for space-based images) are an order of magnitude smaller that the modeling errors. Furthermore, line-of-sight (LOS) structures can introduce a systematic error in the strong lensing modeling (e.g., Host 2012; Bayliss et al. 2014; Jaroszynski & Kostrzewa-Rutkowska 2014; McCully et al. 2014; Giocoli et al. 2016) of up to $\sim 1\farcs4$ on the positions of multiple images (Zitrin et al. 2015). Even distant massive structures in the lens plane have a significant impact on the positions of multiple images (Tu et al. 2008; Limousin et al. 2010). Harvey et al. (2016), by analyzing the *Frontier Field* cluster MACSJ0416 ($z = 0.397$), estimated an error of $\sim 0\farcs5$ on the position of the multiple images when assuming that light traces mass in the SL modeling. However, few studies have investigated their impact on the retrieval of cosmological parameters (Acebron et al. 2017; McCully et al. 2017).

In this paper, we are interested in quantifying the uncertainties in the estimation of cosmological parameters induced by different positional errors of the multiple images. To this end, we analyze the strong lensing effect in the galaxy cluster A1689, as well as in a mock galaxy cluster at $z = 0.5$ generated in a flat ΛCDM cosmology. Because in the CLP case it is possible to obtain tight constraints on its parameters (see Magaña et al. 2015) using the SL methodology proposed by Jullo et al. (2010), in this work we consider popular CPL-like models in which the EoS of dark energy is parameterized as a function of redshift.

The paper is organized as follows. In the next section, Section 2, we introduce the cosmological framework and the parametric dark energy models. In Section 3 we describe the SL data and methodology used to constrain the cosmological parameters of the DE models. In Section 4 we present and discuss the results. Finally, we provide our conclusions in Section 5.

2. Cosmological Framework and Parametric Dark Energy Models

For a homogeneous, isotropic, and flat Friedmann–Lemaître–Robertson–Walker cosmology, the expansion rate of the universe is governed by the Friedmann equation:

$$H^2(z) \equiv \frac{8\pi G}{3} \sum_i \rho_i(z), \tag{1}$$

where $H \equiv \dot{a}/a$ is the Hubble parameter, a is the scale factor of the universe, and ρ_i denotes the energy density for each component in the universe.[5] We consider cold dark matter (m) and radiation (r) components whose dynamics are described by a perfect fluid with EoS $w_m = 0$ and $w_r = 1/3$, respectively. In addition, we also consider a dynamical dark energy (de) whose EoS is parameterized by a $w(z)$ function. In terms of the present values[6] of the density parameters, $\Omega_i \equiv 8\pi G\rho_i/3H(z)^2$, for each component, the Equation (1) reads as:

$$E^2(z) = \Omega_m(1+z)^3 + \Omega_r(1+z)^4 + \Omega_{\rm de} f_{\rm de}(z), \tag{2}$$

where $E(z) = H(z)/H_0$ is the dimensionless Hubble parameter, $\Omega_r = 2.469 \times 10^{-5} h^{-2}(1 + 0.2271 N_{\rm eff})$, with $h = H_0/100$ km s^{-1} Mpc^{-1}, $N_{\rm eff} = 3.04$ is the standard number of relativistic species (Komatsu et al. 2011), and $\Omega_{\rm de}$ can be expressed as $\Omega_{\rm de} = 1 - \Omega_m - \Omega_r$. The function $f_{\rm de}(z)$ is defined as

$$f_{\rm de}(z) \equiv \frac{\rho_{\rm de}(z)}{\rho_{\rm de}(0)} = \exp\left(3\int_0^z \frac{1+w(z)}{1+z} dz\right). \tag{3}$$

Note that, by introducing a $w(z)$ functional form in the integral of the Equation (3), we can obtain an analytical expression for $f_{\rm de}(z)$, and hence for $E(z)$.

In addition, to test whether the constraints for each parametric DE model result in a late cosmic acceleration, we examine the deceleration parameter $q(z)$ defined as:

$$q(z) = -\frac{\ddot{a}(z)a(z)}{\dot{a}^2(z)}. \tag{4}$$

Using Equation (2), we obtain:

$$q(z) = \frac{(1+z)}{E(z)}\frac{dE(z)}{dz} - 1, \tag{5}$$

which expresses the deceleration parameter in terms of the dimensionless Hubble parameter.

2.1. Parametric Dark Energy Models

One alternative to the cosmological constant is to consider a dark energy component that admits a time-dependent EoS. An effective and simple way to study dynamical dark energy models is to assume a phenomenological parameterization of the EoS (Lazkoz et al. 2005; Pantazis et al. 2016). Commonly, this EoS is biparametric and it depends on the scale factor of redshift. The most popular ansatz, denoted CPL parameterization, (introduced and revisited by Chevallier & Polarski 2001; Linder 2003, respectively), is $w(z) = w_0 + w_1 z/(1+z)$, where w_0 is the present value of the EoS and $w_1 = dw(z)/dz|_{z=0}$. In this paper we study five CPL-like EoS parameterizations

[5] Dot stands for the derivative with respect to the cosmic time.
[6] Quantities evaluated at $z = 0$.

(see Magaña et al. 2014; Wang et al. 2016, for details), and we briefly introduce the functional form of these parameterizations as follows:

1. Jassal–Bagla–Padmanabhan (JBP). Jassal et al. (2005a, 2005b) proposed that the dark energy EoS is parameterized by the function

$$w(z) = w_0 + w_1 \frac{z}{(1+z)^2}, \tag{6}$$

which allows rapid variations at low z. The DE has the same EoS at the present epoch and at high redshift, i.e., $w(\infty) = w_0$. By substituting the Equation (6) in Equation (3) we obtain

$$f_{\rm de}(z) = (1+z)^{3(1+w_0)} \exp\left[\frac{3}{2}\frac{w_1 z^2}{(1+z)^2}\right]. \tag{7}$$

2. Barbosa–Alcaniz (BA). Barboza & Alcaniz (2008) considered a parametric EoS for the dark energy component given by

$$w(z) = w_0 + w_1 \frac{z(1+z)}{1+z^2}. \tag{8}$$

This ansatz behaves linearly at low redshifts as $w_0 + w_1$, and $w \to w_0 + w_1 z$ when $z \to \infty$. In addition, $w(z)$ is well-behaved in all epochs of the universe; for instance, the DE dynamics in the future, at $z = -1$, can be investigated without dealing with a divergence. Solving the integral in Equation (3) and using Equation (8), results i:

$$f_{\rm de}(z) = (1+z)^{3(1+w_0)} (1+z^2)^{\frac{3}{2}w_1}. \tag{9}$$

3. Feng–Shen–Li–Li (FSLL, Feng et al. 2012) suggested two dark energy EoS parameterizations given by

$$w(z) = w_0 + w_1 \frac{z}{1+z^2}, \qquad \text{FSLLI} \tag{10}$$

$$w(z) = w_0 + w_1 \frac{z^2}{1+z^2} \qquad \text{FSLLII}. \tag{11}$$

Both functions have the advantage of being divergence-free throughout the entire cosmic evolution, even at $z = -1$. At low redshifts, $w(z)$ behaves as $w_0 + w_1 z$ and $w_0 + w_1 z^2$ for FSLL I and FSLL II, respectively. In addition, when $z \to \infty$, the EoS has the same value, w_0, as the present epoch for FSLL I and $w_0 + w_1$ for FSLL II. Using Equations (10) and (11) to solve Equation (3) leads to

$$f_{\rm de\pm}(z) = (1+z)^{3(1+w_0)} \exp\left[\pm\frac{3w_1}{2}\arctan(z)\right] \times (1+z^2)^{\frac{3}{4}w_1} (1+z)^{\mp\frac{3}{2}w_1}, \tag{12}$$

where f_+ and f_- correspond to FSLL I and FSLL II, respectively.

4. Sendra–Lazkoz (SeLa, Sendra & Lazkoz 2012) improved the CPL parameterization, whose $w_0 - w_1$ parameters are highly correlated and w_1 is poorly constrained by the observational data, introducing new polynomial parameterizations. They are constructed to reduce the parameter correlation, so they can be better constrained by the observations at low redshifts. One of these parameterizations is given by

$$w(z) = -1 + c_1\left(\frac{1+2z}{1+z}\right) + c_2\left(\frac{1+2z}{1+z}\right)^2, \tag{13}$$

where the constants are defined as $c_1 = (16w_0 - 9w_{0.5} + 7)/4$, and $c_2 = -3w_0 + (9w_{0.5} - 3)/4$, and $w_{0.5}$ is the value of the EoS at $z = 0.5$. This $w(z)$ function is well-behaved at higher redshifts as $(-1 - 8w_0 + 9w_{0.5})/2$. By the substitution of Equation (13) into Equation (3), we obtain

$$f_{\rm de}(z) = (1+z)^{\frac{3}{2}(1-8w_0+9w_{0.5})} \times \exp\left[\frac{3z\{w_0(52z+40) - 9w_{0.5}(5z+4) + 7z + 4\}}{8(1+z)^2}\right]. \tag{14}$$

By replacing the $f_{\rm de}(z)$ functions in Equation (1), we obtain an analytical $E(z)$ function for each parametric $w(z)$, which will be used in the following sections to estimate the EoS parameters. Our main purpose is to examine the quality of the $w(z)$ constraints extracted from the SL modeling when different image-position errors are considered.

3. Methodology

3.1. Strong Lensing as a Cosmological Probe

The gravitational lensing effect is produced when the light beam of a background source is deflected by a gravitational lens, i.e., a mass distribution between the source and the observer. We refer to the strong lensing regime when several rings, arcs, or multiples images are observed as a result of the distortion and deflection of the light from a source by a lens. These strong lensing observables offer a powerful and useful tool to not only infer the total matter distribution in astrophysical systems (Jauzac et al. 2014; Monna et al. 2017), but also to provide insights on the total content of the universe, dark matter, and dark energy properties (Golse et al. 2002; Soucail et al. 2004; Jullo et al. 2010; Caminha et al. 2016; Magaña et al. 2015). Here, we use strong lensing measurements in galaxy clusters to constrain the EoS of parametric dark energy models.

Since the strong lensing features depend on the dynamics of the universe via the angular diameter distance between the source, lens and observer, it can be used as a geometric cosmological probe. For any underlying cosmology, the angular diameter distance ratios for two images from different sources define the "family ratio" (see Jullo et al. 2010, for a detailed discussion):

$$\Xi(z_l, z_{s1}, z_{s2}, \boldsymbol{\Theta}) = \frac{D(z_l, z_{s1})}{D(0, z_{s1})}\frac{D(0, z_{s2})}{D(z_l, z_{s2})}, \tag{15}$$

where Θ is the vector of cosmological parameters to be fitted, z_l is the lens redshift, z_{s1} and z_{s2} are the two source redshifts, and $D(z_i, z_f)$ is the angular diameter distance calculated as

$$D(z_i, z_f) = \frac{r(z_i, z_f)}{(1+z_f)}, \tag{16}$$

where $r(z_i, z_f)$, the comoving distance of a source at redshift z_f measured by an observer at redshift z_i, is given by

$$r(z_i, z_f) = \frac{c}{H_0}\int_{z_i}^{z_f}\frac{dz'}{E(z')}. \quad (17)$$

Note that the underlying cosmology in the lens modeling is selected by introducing the $E(z)$ function in the Equation (17). For the parametric DE models, these functions are analytical and $\mathbf{\Theta} = \{\Omega_m, w_0, w_1\}$ ($w_{0.5}$ for the SeLa parameterization) is the free parameter vector.

3.2. Lensing Modeling

To constrain the parameters of the DE models presented in Section 2.1, we use the SL measurements in two galaxy clusters: a real one, Abell 1689, and a simulated one, Ares, from the Frontier Fields Comparison Challenge (Meneghetti et al. 2017).

We performed the SL modeling using the public software LENSTOOL[7] (Kneib et al. 1996; Jullo et al. 2007), in which the DE cosmological models described in Section 2.1 were implemented. LENSTOOL is a ray-tracing code with a Bayesian Markov Chain Monte Carlo sampler that optimizes the model parameters using the positions of the multiply imaged systems. The matter distribution in clusters is modeled in a parametric way and the optimization is performed in the image plane for Abell 1689, as it is more precise (this is different from the analysis by Jullo et al. 2010; Magaña et al. 2015, where the optimization was performed in the source plane). For Ares, the optimization was realized in the source plane, as it is a more complex cluster (more images and cluster members) and this procedure is more computationally efficient. We checked that the results in the image plane were similar for a subset of calculations.

For both Abell 1689 and Ares, each potential (either large or galaxy-scale) is parameterized with the Pseudo Isothermal Elliptical Mass Distribution profile (hereafter PIEMD, Kassiola & Kovner 1993; Elíasdóttir et al. 2007). The density distribution of this profile is given by

$$\rho(r) = \frac{\rho_0}{\left(1+\frac{r^2}{r_{\rm core}{}^2}\right)\left(1+\frac{r^2}{r_{\rm cut}{}^2}\right)}, \quad (18)$$

with a central density ρ_0, a core radius $r_{\rm core}$ and a truncation radius $r_{\rm cut}$. This profile is characterized by two changes in the density slope: it behaves as an isothermal profile within the transition region but the density falls as $\rho \propto r^{-4}$ at large radii. In LENSTOOL, it has the following free parameters: the coordinates x, y; the ellipticity, e; angle position, θ; core and cut radii, $r_{\rm core}$ and $r_{\rm cut}$ and a velocity dispersion, σ. Both clusters were modeled the same way regardless of the considered DE cosmological model.

Abell 1689. A massive cluster at redshift $z = 0.18$, Abell 1689 is one of the most studied strong lenses (see e.g., Limousin et al. 2007, 2013; Diego et al. 2015; Umetsu et al. 2015, and references therein). The first SL modeling was performed by Miralda-Escude & Babul (1995), which already required a bimodal mass distribution for the cluster. It is one of the most X-ray luminous clusters and has a large Einstein radii, $\sim 45''$. A1689 is still the target of recent observations, using MUSE data with which Bina et al. (2016) confirmed or spectroscopically identified new multiple images as well as cluster members.

We refer the reader to Jullo et al. (2010) for a detailed discussion of the modeling of A1689, where a SL parametric model was used to constrain the DE EoS. As we follow-up their approach, we give here a quick overview. Abell 1689 was modeled using the SL features in the deep *HST* observations and extensive ground-based spectroscopic follow-up. The mass distribution was represented as bimodal, with one central and dominant large-scale potential harboring a brightest central cluster galaxy (BCG) in its center. The second large-scale potential was situated in the northeast. Jullo et al. (2010) used 58 cluster galaxies (with $m_K < 18.11$) in the modeling and followed the standard scaling relations. In this work we consider the same catalog as in Jullo et al. (2010), including 28 images from 12 families,[8] all with measured spectroscopic redshifts, spanning a range of $1.15 < z_S < 4.86$.

Ares. A mock galaxy cluster at $z = 0.5$, generated in a flat ΛCDM cosmological model with a matter density parameter $\Omega_m = 0.272$. We model Ares considering all multiple images (242 from 85 sources), all with assumed known spectroscopic redshifts spanning a wide range ($0.91 < z_S < 6.0$). Cluster members are taken from the given simulated catalog up to a magnitude of $m_{F160W} < 22.0$ mag (representing >90% of the total cluster luminosity). Ares is part of an archive of mock clusters that reproduce the characteristics of the *Frontier Fields* observations (the FF-SIMS Challenge, Meneghetti et al. 2017). It was part of a challenge among the strong lensing community to perform, first a blind reconstruction of the mass distribution of the cluster, and then to improve the models after the unblinding of the true mass distribution. The conclusions of this challenge were primarily used to calibrate different modeling techniques. Ares is a semi-analytical cluster created with MOKA[9] by Giocoli et al. (2012). This simulated cluster, a bimodal and realistic cluster, is built with three components: two smooth dark matter triaxial halos, two BCGs and a large number of sub-halos. Dark matter sub-halos are populated using a Halo Occupation Distribution technique and stellar and B-band luminosities are given for all galaxies according to the mass of their sub-halo, as in Wang et al. (2006).

We have modeled Ares as two large-scale potentials and two potentials for the BCGs, whose coordinates are fixed, as well as the ones for the large-scale potentials (see Figure 1 in Acebron et al. 2017). Both components have been parameterized with the PIEMD density profile and corresponds to the model PIEMD—PIEMD in Acebron et al. (2017). The modeling also includes cluster galaxies with $m_{F160W} < 22$ mag (being a more complex cluster, computing time is reduced by introducing a magnitude cut representing >90% of the total cluster luminosity) with masses scaling with luminosity (see Limousin et al. 2005, for further details). Three massive cluster galaxies close to multiple images (see Figure 1 in Acebron et al. 2017) were more carefully modeled (i.e., their parameters deviate from the scaling relations). All multiple images provided were taken into account in the modeling, resulting in an average positional accuracy of $0\farcs66$ and giving tight constraints on the $\Omega_M - w$ space parameter considering a flat ΛCDM cosmology.

To quantify how the cosmological constraints are biased due to systematic effects in the SL modeling, we use different

[7] https://projets.lam.fr/projects/lenstool

[8] A family is the group of images associated with one lensed source.

[9] https://cgiocoli.wordpress.com/research-interests/moka/

Table 1
JBP Mean Fit Parameters Obtained for Both Galaxy Clusters' SL Data

Cluster name	Error in the pos. ($''$)	$\chi^2_{\rm red}$	rms ($''$)	FOM	Ω_m	w_0	w_1
Abell 1689	0.25	11.37	0.54	15.09	$0.47^{+0.04}_{-0.06}$	$-1.29^{+1.04}_{-0.01}$	$-6.46^{+4.88}_{-0.33}$
Ares		2.73	0.59	127.92	$0.37^{+0.12}_{-0.11}$	$-0.82^{+0.11}_{-0.11}$	$-0.14^{+0.36}_{-0.04}$
Abell 1689	0.5	3.14	0.64	8.13	$0.46^{+0.08}_{-0.08}$	$-1.11^{+1.20}_{-0.04}$	$-6.14^{+5.49}_{-0.07}$
Ares		0.78	0.65	11.83	$0.46^{+0.06}_{-0.11}$	$-0.90^{+0.60}_{-0.49}$	$-1.77^{+0.07}_{-3.01}$
Abell 1689	1.0	0.95	0.88	4.15	$0.43^{+0.18}_{-0.12}$	$-1.07^{+0.69}_{-0.60}$	$-5.09^{+3.07}_{-3.40}$
Ares		0.77	0.94	20.46	$0.33^{+0.06}_{-0.06}$	$-1.06^{+0.83}_{-0.43}$	$-5.81^{+3.41}_{-3.16}$
			Complementary probes				
$H(z)$	⋯	0.54	⋯	354.12	$0.26^{+0.01}_{-0.02}$	$-0.88^{+0.27}_{-0.19}$	$-0.70^{+1.83}_{-2.59}$
SN Ia	⋯	0.98	⋯	75.51	$0.32^{+0.05}_{-0.10}$	$-0.70^{+0.19}_{-0.18}$	$-4.44^{+3.40}_{-3.49}$
BAO	⋯	2.17	⋯	646.43	$0.25^{+0.02}_{-0.02}$	$-1.34^{+0.26}_{-0.15}$	$0.43^{+1.13}_{-1.99}$
CMB	⋯	58.8	⋯	8207.46	$0.32^{+0.002}_{-0.002}$	$-0.69^{+0.50}_{-0.68}$	$-4.54^{+4.26}_{-3.66}$

Note. The columns give the reduced $\chi^2_{\rm red}$, rms in the image plane (in arcseconds) and the mean values for Ω_m, w_0, w_1 with 68% confidence level errors. The mean values estimated with $H(z)$, SN Ia, BAO, and CMB data are also provided.

image-positional errors, $\delta_{\rm pos}$, and compare the resulting DE parameter estimations. For each parametric DE model and for both Abell 1689 and Ares, we carry out three runs considering the following errors for the multiple images positions: $0\farcs25$, $0\farcs5$, and $1\farcs0$. These values are chosen arbitrarily but they intend to cover the range of values of systematic uncertainties reported by different authors (Zitrin et al. 2015; Harvey et al. 2016). For instance, the observations indicate uncertainties on the image positions $\sim 0\farcs06$ (Grillo et al. 2015, see also Chirivì et al. 2018), which is almost one order of magnitude less than our smaller error. Nevertheless, the same authors increase this error in the modeling up to six times, i.e., $0\farcs4$, to take into account systematics due to the LOS structures and small dark matter clumps. Although an error of $0\farcs5$ is in agreement with predictions of the effects of matter density fluctuations along the LOS (Host 2012; Caminha et al. 2016), other authors claim that $1\farcs4$ is the proper error to account for these systematics in lens modeling (e.g., Zitrin et al. 2012). Finally, Chirivì et al. (2018) proposed using different errors in the range $0\farcs2$–$0\farcs4$ for different images. In order to consider all these possible effects, we propose $0\farcs25$ as the minimum error in the position of images and increase it two times in each run.

The best-fitting model parameters are found by minimizing the distance between the observed and model-predicted positions of the multiple images. To assess the goodness of the lens model fit we examine the reduced chi-squared, $\chi^2_{\rm red}$ (see Jullo et al. 2007 for details on how it is calculated in the source and image plane). We also use the root mean square between the observed and predicted positions of the multiple images from the modeling, computed as

$$\mathrm{rms} = \sqrt{\frac{1}{N}\sum_{i=1}^{n} |\theta_i^{\rm obs} - \theta_i^{\rm pred}|^2}\,, \tag{19}$$

where $\theta_i^{\rm obs}$ and $\theta_i^{\rm pred}$ are the observed and model-predicted positions of the multiples images and N is the total number of images. Although both estimators are widely used to compare the goodness of the fit of the cluster parameters among different lens models (e.g., Jullo et al. 2010; Caminha et al. 2016; Limousin et al. 2016), they are less sensitive to the cosmological parameters. A reliable tool to measure the goodness of fit for the cosmological constraints is the Figure-of-Merit (FOM, Wang 2008) given by

$$\mathrm{FoM} = \frac{1}{\sqrt{\det \mathrm{Cov}(f1, f2, f3, \ldots)}}, \tag{20}$$

where $\mathrm{Cov}(f1, f2, f3, \ldots)$ is the covariance matrix of the cosmological parameters f_i. This indicator (Equation (20)) is a generalization of those proposed by Albrecht et al. (2006) and the larger values imply stronger constraints on the cosmological parameters, since the indicator corresponds to a smaller error ellipse.

4. Results

In this section we present, for each cosmological model, the constraints from the strong lensing measurements of Ares and Abell 1689, as well as those from other complementary probes ($H(z)$, SNe Ia, BAO, and CMB, see Appendix A). The mock Ares cluster has the advantage of being able to directly compare and validate the cosmological constraints from the SL technique with the fiducial cosmology i.e., the ΛCDM with $\Omega_m = 0.272$.

For each cosmological model, the cluster model parameters and the cosmological parameters are simultaneously optimized with the LENSTOOL software with 80,000 MCMC steps. For the complementary probes, we carry out the EMCEE python module (Foreman-Mackey et al. 2013) employing 500 walkers, 2500 burn-in phase steps, and 7500 MCMC steps to guaranty the convergence. In all our estimations, we have adopted a dimensionless Hubble constant $h = 0.70$.

Tables 1–5 show the mean parameters obtained after optimization for both Abell 1689, Ares and each cosmological model (JBP, BA, FSLL I, FSLL II, and SeLa). For each positional uncertainty considered, we present the $\chi^2_{\rm red}$ and the rms in the image plane, as well as the mean values obtained for the cosmological parameters fitted, Ω_m, $w_{0,}$ and w_1, with the 68% uncertainties. The same tables also give the mean values for the DE parameters obtained from the complementary probes. The best-fit and 2D confidence contours for the cosmological parameters were computed using the python module Getdist.[10]

[10] It can be download at https://github.com/cmbant/getdist.

Table 2
Mean Fit Parameters for the BA Parameterization

Cluster name	Error in the pos. (″)	$\chi^2_{\rm red}$	rms (″)	FOM	Ω_m	w_0	w_1
Abell 1689	0.″25	11.40	0.54	13.57	$0.47^{+0.05}_{-0.06}$	$-1.32^{+0.98}_{-0.01}$	$-6.28^{+5.31}_{-0.07}$
Ares		2.69	0.59	5.25	$0.27^{+0.46}_{-0.01}$	$-0.89^{+0.16}_{-0.48}$	$0.09^{+0.91}_{-1.10}$
Abell 1689	0.″5	3.15	0.64	6.22	$0.44^{+0.08}_{-0.10}$	$-1.15^{+1.20}_{-0.02}$	$-5.22^{+6.17}_{-0.57}$
Ares		0.80	0.65	8.25	$0.20^{+0.36}_{-0.01}$	$-1.10^{+0.31}_{-0.24}$	$0.36^{+0.16}_{-1.81}$
Abell 1689	1.″0	0.94	0.89	3.26	$0.41^{+0.17}_{-0.15}$	$-1.08^{+1.26}_{-0.02}$	$-4.49^{+0.62}_{-7.69}$
Ares		0.33	0.93	6.91	$0.26^{+0.31}_{-0.0}$	$-1.37^{+0.31}_{-0.24}$	$-1.88^{+0.18}_{-6.28}$
			Complementary probes				
$H(z)$	⋯	0.57	⋯	405.21	$0.25^{+0.02}_{-0.08}$	$-0.90^{+0.13}_{-0.12}$	$0.01^{+0.43}_{-0.85}$
SN Ia	⋯	0.98	⋯	70.47	$0.37^{+0.04}_{-0.09}$	$-0.78^{+0.22}_{-0.17}$	$-3.24^{+2.37}_{-3.14}$
BAO	⋯	2.25	⋯	1541.69	$0.26^{+0.02}_{-0.02}$	$-1.23^{+0.18}_{-0.16}$	$-0.23^{+0.52}_{-0.69}$
CMB	⋯	58.8	⋯	3492.21	$0.32^{+0.002}_{-0.002}$	$-0.63^{+0.45}_{-0.67}$	$-2.24^{+2.18}_{-1.82}$

Table 3
Mean Fit Parameters for the FSLL I Parameterization

Cluster name	Error in the pos. (″)	$\chi^2_{\rm red}$	rms (″)	FOM	Ω_m	w_0	w_1
Abell 1689	0.″25	11.53	0.54	12.67	$0.46^{+0.05}_{-0.06}$	$-1.39^{+0.93}_{-0.04}$	$-6.60^{+5.04}_{-0.07}$
Ares		2.70	0.59	168.03	$0.17^{+0.22}_{-0.03}$	$-0.99^{+0.24}_{-0.16}$	$0.48^{+0.29}_{-0.72}$
Abell 1689	0.″5	3.07	0.64	4.10	$0.42^{+0.09}_{-0.12}$	$-1.17^{+1.08}_{-0.21}$	$-4.75^{+0.14}_{-8.73}$
Ares		0.80	0.65	11.29	$0.23^{+0.36}_{-0.02}$	$-1.36^{+0.60}_{-0.15}$	$0.79^{+0.08}_{-3.00}$
Abell 1689	1.″0	0.93	0.89	3.34	$0.40^{+0.17}_{-0.15}$	$-1.15^{+1.07}_{-0.16}$	$-4.99^{+6.08}_{-1.12}$
Ares		0.33	0.92	8.03	$0.27^{+0.32}_{-0.01}$	$-1.45^{+0.97}_{-0.15}$	$-1.89^{+0.13}_{-7.13}$
			Complementary probes				
$H(z)$	⋯	0.48	⋯	268.56	$0.25^{+0.02}_{-0.06}$	$-0.95^{+0.19}_{-0.15}$	$0.14^{+1.03}_{-1.46}$
SN Ia	⋯	0.98	⋯	71.57	$0.36^{+0.05}_{-0.10}$	$-0.74^{+0.22}_{-0.18}$	$-3.77^{+2.77}_{-3.37}$
BAO	⋯	2.13	⋯	1014.38	$0.24^{+0.02}_{-0.02}$	$-1.40^{+0.25}_{-0.19}$	$0.51^{+0.92}_{-1.24}$
CMB	⋯	58.8	⋯	5455.18	$0.32^{+0.002}_{-0.002}$	$-0.69^{+0.50}_{-0.68}$	$-2.86^{+3.05}_{-2.54}$

Table 4
Mean Fit Parameters for the FSLL II Parameterization

Cluster name	Error in the pos. (″)	$\chi^2_{\rm red}$	rms (″)	FOM	Ω_m	w_0	w_1
Abell 1689	0.″25	11.90	0.54	19.78	$0.41^{+0.05}_{-0.06}$	$-1.61^{+0.54}_{-0.03}$	$-5.59^{+6.82}_{-0.09}$
Ares		2.71	0.59	50.04	$0.19^{+0.33}_{-0.01}$	$-0.81^{+0.06}_{-0.10}$	$0.18^{+0.13}_{-0.80}$
Abell 1689	0.″5	3.17	0.64	7.96	$0.38^{+0.09}_{-0.10}$	$-1.45^{+0.57}_{-0.26}$	$-4.81^{+7.24}_{-0.29}$
Ares		0.79	0.65	8.74	$0.38^{+0.15}_{-0.21}$	$-1.00^{+0.25}_{-0.44}$	$-0.64^{+0.38}_{-4.69}$
Abell 1689	1.″0	0.94	0.89	3.31	$0.35^{+0.20}_{-0.14}$	$-1.29^{+0.70}_{-0.31}$	$-4.78^{+7.57}_{-0.10}$
Ares		0.32	0.92	9.50	$0.28^{+0.06}_{-0.14}$	$-1.35^{+0.29}_{-0.54}$	$-2.11^{+0.50}_{-7.14}$
			Complementary probes				
$H(z)$	⋯	0.56	⋯	164.36	$0.26^{+0.02}_{-0.06}$	$-0.92^{+0.11}_{-0.10}$	$-0.30^{+0.92}_{-2.12}$
SN Ia	⋯	0.98	⋯	71.30	$0.32^{+0.04}_{-0.11}$	$-0.98^{+0.15}_{-0.15}$	$-4.34^{+3.90}_{-3.86}$
BAO	⋯	2.21	⋯	530.10	$0.27^{+0.02}_{-0.02}$	$-1.19^{+0.12}_{-0.10}$	$-1.34^{+1.23}_{-1.91}$
CMB	⋯	58.8	⋯	2702.46	$0.32^{+0.002}_{-0.002}$	$-0.87^{+0.22}_{-0.34}$	$-4.96^{+4.01}_{-3.51}$

4.1. Effect of Image-position Error on the Cosmological Parameters

The positional error for the multiple images plays a key role in both the lens modeling and the cosmological parameter estimation (Magaña et al. 2015; Caminha et al. 2016; Limousin et al. 2016). As mentioned in Section 1, a large error could take into account other sources of uncertainties in the SL measurements, such as systematic errors due to foreground and background structures (D'Aloisio & Natarajan 2011; Host 2012; Bayliss et al. 2014; Zitrin et al. 2015), or the cluster's environment (Acebron et al. 2017; McCully et al. 2017). As a first test, we constrain the JBP cosmological parameters from Ares SL data with an image-positional error $\delta_{\rm pos} = 1''$. For this run (see Table 1), we obtain $\chi^2_{\rm red} = 0.77$ and rms $= 0.''94$, both criteria indicating a good fit for the cluster parameters. When modeling Ares using smaller positional uncertainties ($\delta_{\rm pos} = 0.''25, 0.''5$), the $\chi^2_{\rm red}$ values point out a poor model fit. The left panel of Figure 1 illustrates the comparison of the $\Omega_m - w_0$ confidence contours obtained with different positional uncertainties for the JBP model using Ares SL data. This figure clearly shows that increasing the positional uncertainty translates to an enlargement of the confidence contours and a systematic shift in the Ω_{m0} estimation toward the fiducial value. However, the χ^2 statistical estimator also depends on the uncertainty considered for the position of the multiple images. Thus, the change in the shape of the confidence contours at

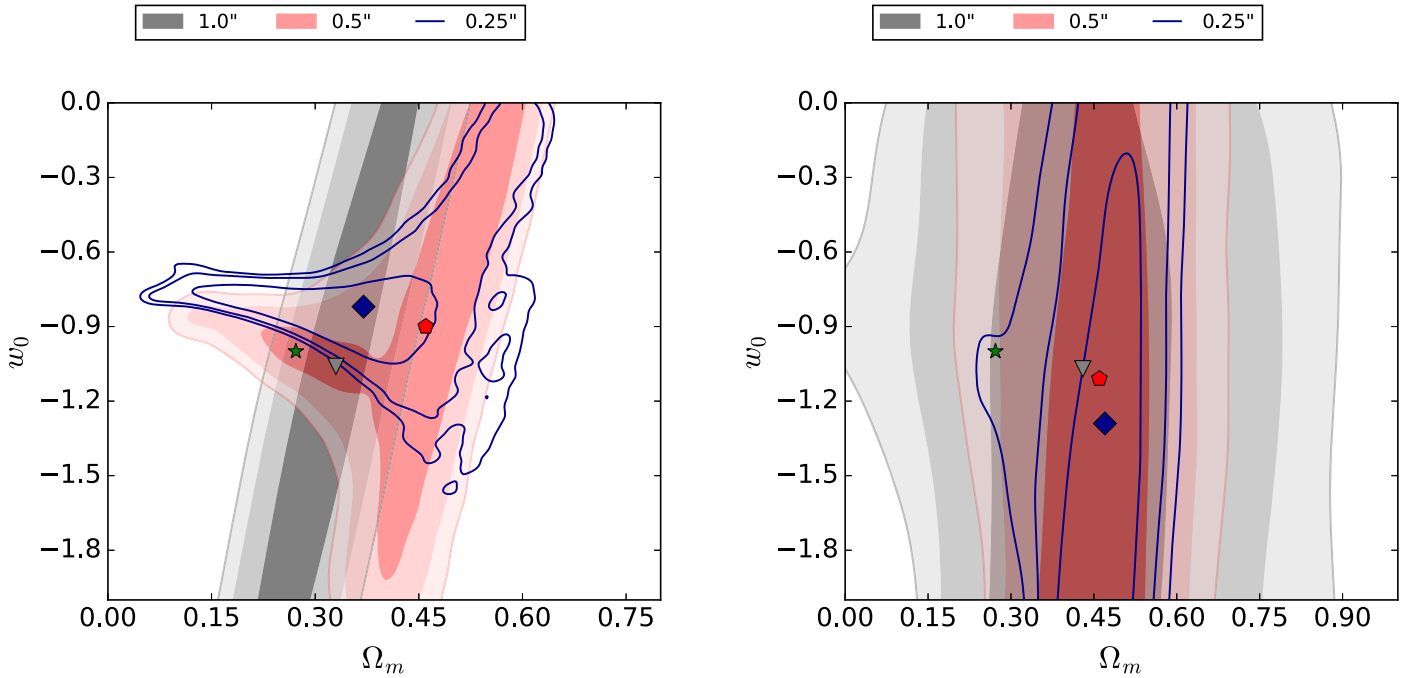

Figure 1. Comparison of the constraints on the Ω_m–w_0 parameters for Ares (left panel) and Abell 1689 (right panel) when considering several positional uncertainties ($\delta_{\rm pos}$) in the SL modeling for the JBP parameters. The star indicates the reference fiducial values. The mean values when $\delta_{\rm pos}$ is $0\farcs25$, $0\farcs5$, and $1\farcs0$ are represented by the diamond, pentagon, and triangle respectively.

Table 5
Mean Fit Parameters for the SeLa Parameterization

Cluster name	Error in the pos. ($''$)	$\chi^2_{\rm red}$	rms ($''$)	FOM	Ω_m	w_0	$w_{0.5}$
Abell 1689	$0\farcs25$	11.66	0.54	43.94	$0.42^{+0.07}_{-0.10}$	$-1.23^{+0.94}_{-0.24}$	$0.61^{+0.38}_{-1.57}$
Ares		6.01	4.80	33.84	$0.80^{+0.06}_{-0.09}$	$-1.04^{+1.25}_{-0.08}$	$0.38^{+0.65}_{-1.56}$
Abell 1689	$0\farcs5$	3.06	0.64	25.21	$0.41^{+0.11}_{-0.09}$	$-1.18^{+1.06}_{-0.13}$	$-0.54^{+0.02}_{-1.96}$
Ares		1.57	1.11	25.09	$0.66^{+0.12}_{-0.09}$	$-1.26^{+1.07}_{-0.01}$	$-0.59^{+0.14}_{-1.83}$
Abell 1689	$1\farcs0$	0.93	0.90	12.67	$0.46^{+0.04}_{-0.05}$	$-1.39^{+0.73}_{-0.44}$	$-6.60^{+3.87}_{-2.44}$
Ares		0.48	1.06	23.61	$0.41^{+0.16}_{-0.10}$	$-1.16^{+1.17}_{-0.04}$	$0.49^{+0.79}_{-1.40}$
			Complementary probes				
$H(z)$	⋯	0.55	⋯	703.29	$0.25^{+0.02}_{-0.07}$	$-0.90^{+0.14}_{-0.12}$	$-1.01^{+0.31}_{-0.36}$
SN Ia	⋯	0.98	⋯	111.75	$0.37^{+0.05}_{-0.09}$	$-0.73^{+0.28}_{-0.18}$	$-2.64^{+1.23}_{-1.57}$
BAO	⋯	9.95	⋯	377.94	$0.23^{+0.04}_{-0.08}$	$-1.04^{+0.28}_{-0.23}$	$-1.11^{+0.55}_{-0.37}$
CMB	⋯	58.8	⋯	1004.52	$0.32^{+0.002}_{-0.002}$	$-0.56^{+0.40}_{-0.54}$	$-1.98^{+0.51}_{-0.50}$

$0\farcs25$ could be explained by the underestimation of the image-position uncertainties. For instance, Acebron et al. (2017) measured an average positional accuracy of $0\farcs66$ for Ares using a strong lens model under the standard cosmology. Therefore, in the case of our $w(z)$ parameterizations, we would expect reasonable Ares models when the image-position errors are roughly similar to the average positional accuracy obtained (i.e., $\sim 0\farcs5$–$1''$). We confirm that more statistically significant constraints for the lens (cluster) model are obtained for larger errors, i.e., the reduced $\chi^2_{\rm red}$ value trends to one. This same trend is recovered for the JBP, FSLL I, FSLL II, and SeLa parameterizations (see Tables 2–5).

The main indicator of the quality of the cosmological constraints is provided by the FOM values. Although there is not a clear trend in FOM versus $\delta_{\rm pos}$, the strong constraints for the BA, FSLL I, FSLL II, and SeLa parameters are obtained when $\delta_{\rm pos} = 0\farcs25$. However, this uncertainty can lead to a poor cluster model. Moreover, this error provide SL confidence contours that are only consistent within the 3σ confidence levels like those obtained from the other cosmological tests. The optimum fit is obtained as a compromise between those $\chi_{\rm red}$ and rms values that provide a good lens model and the FOM value that gives cosmological constraints that are also in agreement with other probes. Thus, in the following, we discuss the parameter estimation for the case in which those criteria are fulfilled (i.e., $\delta_{\rm pos} = 1''$, see Appendix B).

4.2. $w(z)$ Parameter Estimations from SL in Abell 1689

In general, for all models, we found that the SL technique using Abell 1689 data provides better Ω_m constraints than the ones on the EoS parameters and confirm our previous result: a larger error ($\delta_{\rm pos} = 1''$) provides more significant constraints for the cluster parameters, i.e., $\chi_{\rm red} \sim 1$, and reasonable rms values. As in the Ares case, the right panel of the Figure 1 shows that increasing $\delta_{\rm pos}$ is translated into an enlargement of the confidence contours and a systematic shift in the Ω_{m0} estimation toward the fiducial value. In addition, although this uncertainty produces the lowest

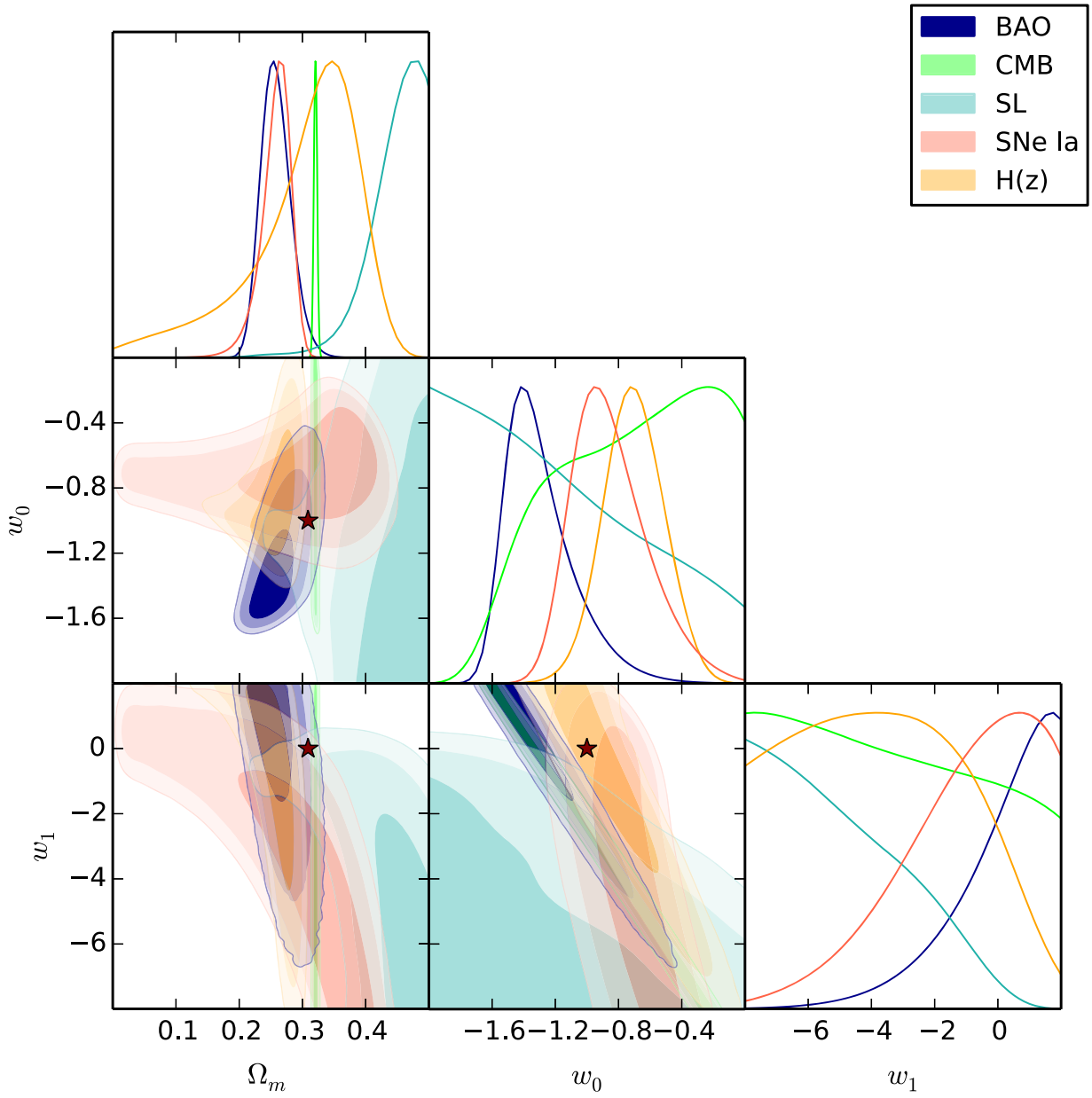

Figure 2. Confidence contours (1σ, 2σ, 3σ) and the marginalized one-dimensional posterior probability distributions on the Ω_m, w_0, and w_1 parameters for the cosmological model JBP for Abell 1689 with $\delta_{\rm pos} = 0\farcs25$. The star indicates the cosmological parameters as constrained by Planck Collaboration et al. (2016b) for a $\Lambda_{\rm CDM}$ cosmology.

FOM values (i.e., less significant cosmological parameters) for all $w(z)$ parameterizations, the confidence contours are in complete agreement with those of the other probes. Figures 2–4 show the 1σ, 2σ, and 3σ confidence contours and the marginalized one-dimensional posterior probability distributions on the Ω_m, w_0, and w_1 parameters for the cosmological model JBP using Abell 1689 SL data for each positional uncertainty considered. We note again that when the error in the image position is increased, the Ω_m–w_0 and Ω_m–w_1 (or w_0–w_1) confidence contours shift toward the left (upper) region, where the confidence contours from BAO, CMB, SNe Ia, and $H(z)$ probes are overlapped. This same trend is recovered for the BA, FSLL I, FSLL II, and SeLa parameterizations (their confidence contours are provided in Figures 6–9 of the Appendix B).

On the other hand, the w_0 and w_1 mean values for the five $w(z)$ parameterizations could suggest a dynamical EoS, which can be associated with thawing or freezing quintessence DE (Pantazis et al. 2016). Nevertheless, all our EoS constraints are consistent with the cosmological constant, i.e., $w_0 = -1$, and $w_1 = 0$, within the 3σ confidence level. In addition, there is no significant difference among the $\chi^2_{\rm red}$ and rms values for different $w(z)$ parameterizations. Therefore, any parametric DE model could be the source of the late cosmic acceleration. We confirm this result in the left panel of Figure 5, which shows the reconstruction of the cosmological evolution for each parameterization using the mean values obtained from the SL modeling in Abell 1689 when $\delta_{\rm pos} = 1''$ is considered.

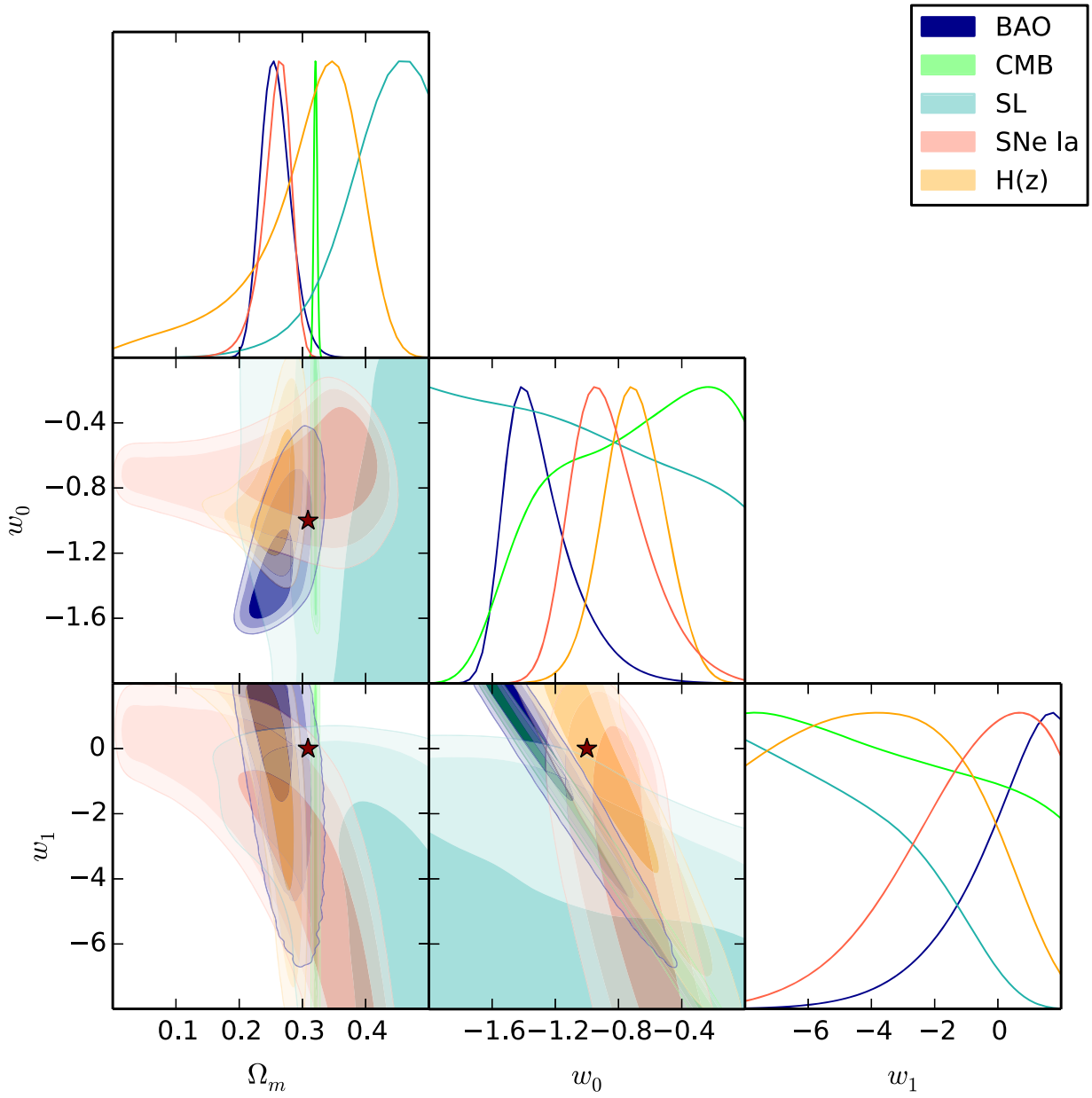

Figure 3. Confidence contours (1σ, 2σ, 3σ) and the marginalized one-dimensional posterior probability distributions on the Ω_m, w_0, and w_1 parameters for the cosmological model JBP for Abell 1689 with $\delta_{\rm pos} = 0\farcs5$. The star indicates the cosmological parameters as constrained by Planck Collaboration et al. (2016b) for a $\Lambda_{\rm CDM}$ cosmology.

4.3. Deceleration Parameter

The cosmological behavior of the deceleration parameter (Equation (5)) is an important test to know whether a DE model is able to handle the late cosmic acceleration. The right panels of Figure 5 show the reconstructed $q(z)$ evolution for each parameterization obtained from Abell 1689 SL data when the multiple image-positional error is $1''$. We also have propagated its error within the 1σ confidence level using a Monte Carlo approach. Note that the five cosmological models predict an accelerating expansion at late times. The transition redshifts, i.e., when the universe passes from an decelerated phase to an accelerated one, are $z_t = 0.44^{+0.21}_{-0.17}$, $0.44^{+0.17}_{-0.12}$, $0.45^{+0.18}_{-0.13}$, $0.50^{+0.22}_{-0.24}$, $0.34^{+0.07}_{-0.04}$ for the JBP, BA, FSLL I, FSLL II, and SeLa parameterizations, respectively. Furthermore, the $q(z)$ shape for each parameterization is consistent with that of the cosmological constant within the 1σ confidence level.

5. Conclusions

Several recent studies have shown that dark energy could deviate from a cosmological constant (Ferreira et al. 2017; Zhao et al. 2017). A simple way to investigate such alternative dark energy models is to parameterize the dark energy EoS as a function of redshift. In order to elucidate the nature of dark energy, numerous parameterizations have been proposed (see, for instance, Pantazis et al. 2016, and references therein). The typical tests to constrain cosmological parameters use SNe Ia, $H(z)$, BAO, and CMB distance posterior measurements. Nevertheless, some of them could provide biased constraints because either the data or the test fitting formulae are derived assuming an underlying standard cosmology (see Appendix A). Furthermore, new complementary techniques could break the degeneracy between parameters and obtain stringent constraints that could help us distinguish the nature of dark energy.

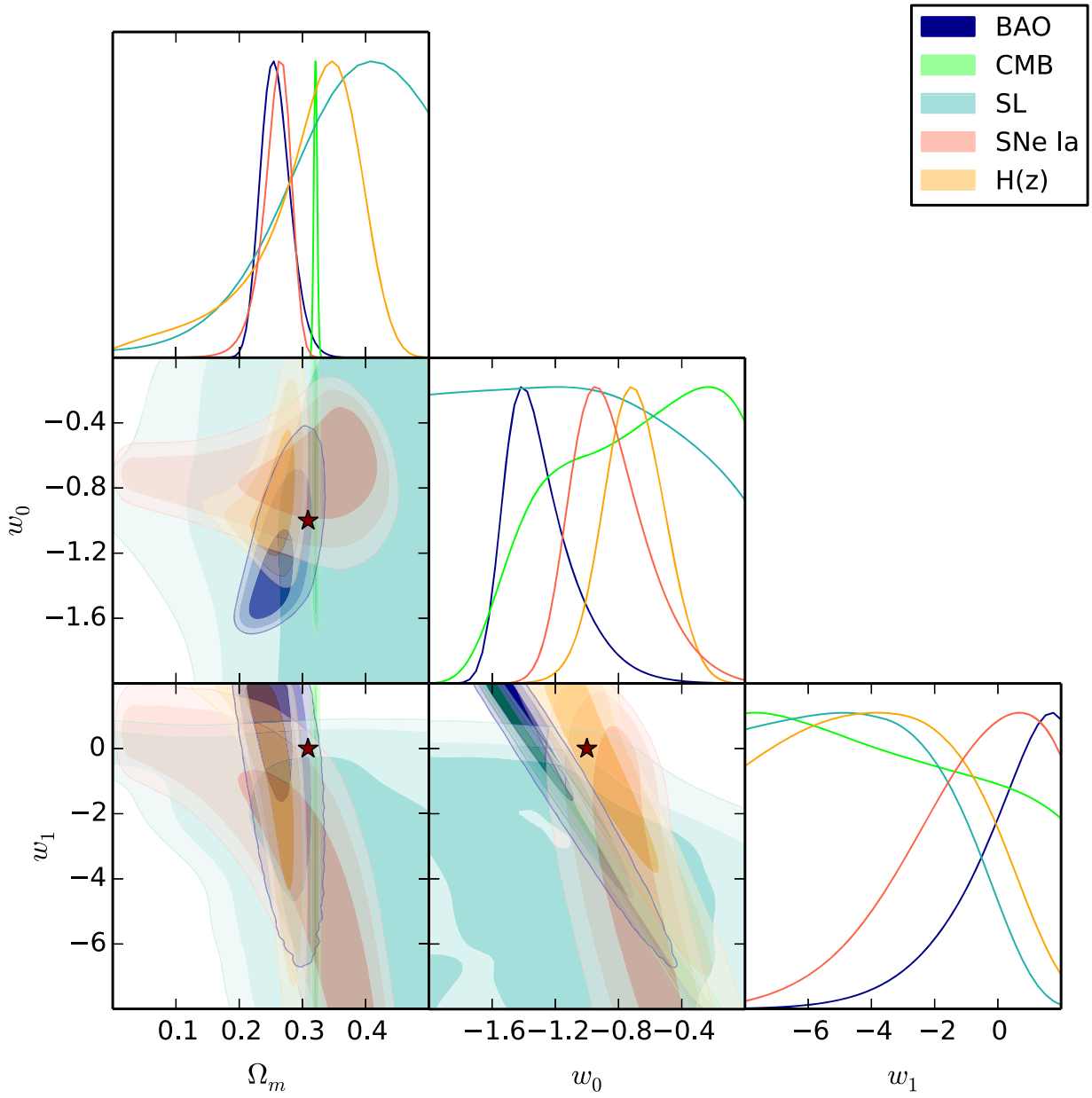

Figure 4. Confidence contours (1σ, 2σ, 3σ) and the marginalized one-dimensional posterior probability distributions on the Ω_m, w_0, and w_1 parameters for the cosmological model JBP for Abell 1689 with $\delta_{\rm pos} = 1\farcs0$. The star indicates the cosmological parameters as constrained by Planck Collaboration et al. (2016b) for a $\Lambda_{\rm CDM}$ cosmology.

In this paper, which is the first in a series, we investigate a promising technique to study alternative cosmological models and to constrain their parameters using the strong lensing features in galaxy clusters. This method has the advantage of providing constraints which are not biased due to an underlying cosmology.

We have considered five popular biparametric CPL-like ansatzes—JBP, BA, FSLL I, FSLL II, and SeLa—and constrained their parameters using the SL data in a real galaxy cluster, Abell 1689, and a simulated one, Ares. We implemented these $w(z)$ parameterizations in the LENSTOOL code, which uses an MCMC algorithm to simultaneously constrain the lens model and the $w(z)$ parameters. In addition, we have considered three different image-positional errors to quantify how the cosmological constraints are affected by these uncertainties in the lens modeling. In general, we found that the SL technique provides competitive constraints on the $w(z)$ parameters in comparison with the common cosmological tests. Moreover, when increasing the image-positional error (from $0\farcs5$ to $1\farcs0$), we find that systematic biases with respect to the known input cosmological values in the simulated cluster decrease. After taking this calibration into account in the real data, our SL constraints are consistent with those obtained from other probes.

In summary, we have exploited the strong lensing modeling in galaxy clusters as a cosmological probe. Although we have measured competitive constraints on the $w(z)$ parameters, further analysis on the galaxy clusters and their environment is needed to improve the strong lensing modeling and hence to more tightly estimate cosmological parameters. In forthcoming

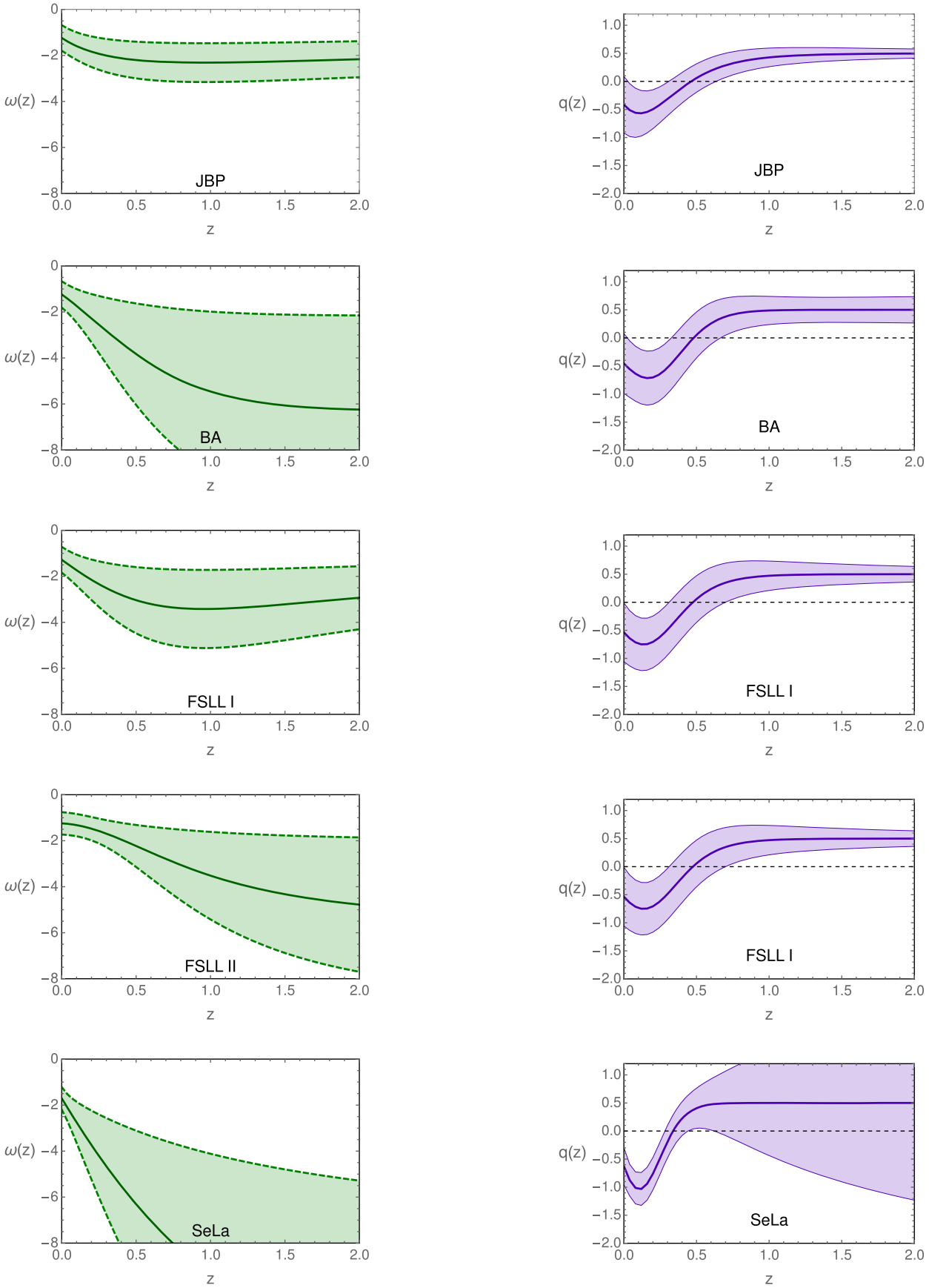

Figure 5. Reconstructed equation of state (left panel) and deceleration parameter (right panel) vs. redshift for each $w(z)$ parameterization using the mean values obtained from SL data in Abell 1689 with an image-position error of $1\overset{''}{.}0$. The shadow regions show the 1σ region calculated with an MCMC error propagation approach using the SL posterior constraints.

papers, we will test this method to constrain the parameters of other cosmological scenarios such as, for instance, those considering interactions in the dark sector.

We thank the anonymous referee for thoughtful remarks and suggestions. J.M. acknowledges the support from CONICYT/FONDECYT project 3160674 and is thankful for the hospitality of the staff of LAM, where part of this work was done. This work has been carried out thanks to the support of the OCEVU Labex (ANR-11-LABX-0060) and the A*MIDEX project (ANR-11-IDEX-0001-02) funded by the "Investissements d'Avenir" French government program managed by the ANR.

This work was granted access to the HPC resources of Aix-Marseille Université financed by the project Equip@Meso (ANR-10-EQPX-29-01) of the program "Investissements d'Avenir" supervised by the Agence Nationale pour la Recherche. This research has been carried out thanks to PROGRAMA UNAM-DGAPA-PAPIIT IA102517. T.V. thanks the staff of the Instituto de Física y Astronomía of the Universidad de Valparaíso. M.L. acknowledges the support from Centre national de la recherche scientifique (CNRS), Programme National de Cosmologie et Galaxies (PNCG) and CNES.

Appendix A
Additional Cosmological Data

We compare the constraints obtained from the strong lensing modeling with those from BAO, CMB, SNe Ia, and $H(z)$ cosmological probes. In the following we describe briefly these cosmological data, for further details on how their FOM is constructed (see Magaña et al. 2015, 2017 and references therein).

A.1. BAO

Large-scale galaxy surveys offer the possibility of measuring the signatures of BAOs, which have typical length scales imprinted on both photons and baryons by the propagation of sound waves in the primordial plasma of the universe. This signal, i.e., the sound horizon at the drag epoch, $r_s(z_d)$, is a standard ruler that can be used to test alternative cosmologies. To complement our SL constraints, we use the following 9 BAO points (see Magaña et al. 2017, and references therein) to constrain the $w(z)$ functions as follows:

1. 6dFGS. $z = 0.106$, $dz \equiv \frac{r_s(z_d)}{D_V(z)} = 0.336 \pm 0.015$, where $D_V(z) = \frac{1}{H_0}\left[(1+z)^2 D(z)^2 \frac{cz}{E(z)}\right]^{1/3}$.
2. WiggleZ. $z = [0.44, 0.6, 0.73]$, $dz = [0.0870 \pm 0.0042, 0.0672 \pm 0.0031, 0.0593 \pm 0.0020]$.
3. SDSS DR7 $z = 0.15{,}0.2239 \pm 0.0084$.
4. SDSS-III BOSS DR11 (a). $z = [0.32, 0.57]$, $dz = [0.1181 \pm 0.0022, 0.0726 \pm 0.0007]$.
5. SDSS-III BOSS DR11 (b). $z = [2.34, 2.36]$, $\frac{D_H(z)}{r_s(z_d)} = [9.18 \pm 0.28, 9.00 \pm 0.3]$, where $D_{H(z)} = c/H_0 E(z)$.

It is worth noting that $r_s(z_d)$ depends on the underlying cosmology, which is commonly the ΛCDM model. Moreover, the z_d formulae employed in the BAO fitting (Eisenstein & Hu 1998) were calculated for the standard cosmology. Thus, the BAO constraints could be biased due to the standard cosmology.

A.2. Distance Posteriors from CMB Planck 2015 Measurements

The information of the CMB acoustic peaks can be compressed in to three quantities, their distance posteriors: the acoustic scale, l_A, the shift parameter, R, and the decoupling redshift, z_*. Several authors have proved that these quantities are almost independent of the input DE models (Wang et al. 2012). Thus, to constrain the $w(z)$ parameters we use the following distance posteriors for a flat wCDM, estimated by Neveu et al. (2017) from Planck 2015 measurements: $l_A^{\rm obs} = 301.787 \pm 0.089$, $R^{\rm obs} = 1.7492 \pm 0.0049$, $z_*^{\rm obs} = 1089.99 \pm 0.29$.

It is worth noting that the fitting formulae for these quantities (Hu & Sugiyama 1996; Bond et al. 1997) are calculated for the standard model; however, we assume that they are valid in dynamical DE models.

A.3. SNe Ia

Since Type Ia Supernovae are standard candles, i.e., their light curves have the same shape after a standardization process, they have been used to measure cosmological parameters. Indeed, the apparent cosmic accelerating expansion was observed through a Hubble diagram of distant SN Ia. As a complementary test, we consider the compilation by Ganeshalingam et al. (2013) that contains 586 data points of the modulus distance, μ, in the redshift range $0.01 < z < 1.4$, which includes 91 points from the Lick Observatory Supernova Search SN Ia observations.

A.4. H(z) Measurements

The Hubble parameter at different redshifts provides a direct measurement of the expansion rate of the universe. Several authors have estimated the observational Hubble data using different techniques: from clustering or BAO peaks (see for instance, Gaztanaga et al. 2009) and from cosmic chronometers (Jimenez & Loeb 2002). Here, we use the same sample used by Magaña et al. (2017), which contains 34 data points in the redshift range $0.07 < z < 2.36$. Although some of the $H(z)$ points were estimated from BAO data, we assume that there is no correlation between them. It is worth noting that the $H(z)$ points obtained from BAO could yield to biased constraints due to the underlying (ΛCDM) cosmology on $r_s(z_d)$.

Appendix B
Confidence Contours for the BA, FSLL I, FSLL II, and SeLa Parameterizations

Figures 6–9 show the confidence contours of the constraints obtained from SL in Abell 1689 with an image-position error of $1.0''$ for the BA, FSLL I, FSLL II, and SeLa parameterizations, respectively. The confidence contours obtained from BAO, CMB, SNe Ia, and $H(z)$ are also shown. Notice that for these parameterizations, the SL confidence contours are in complete agreement with those of the other probes.

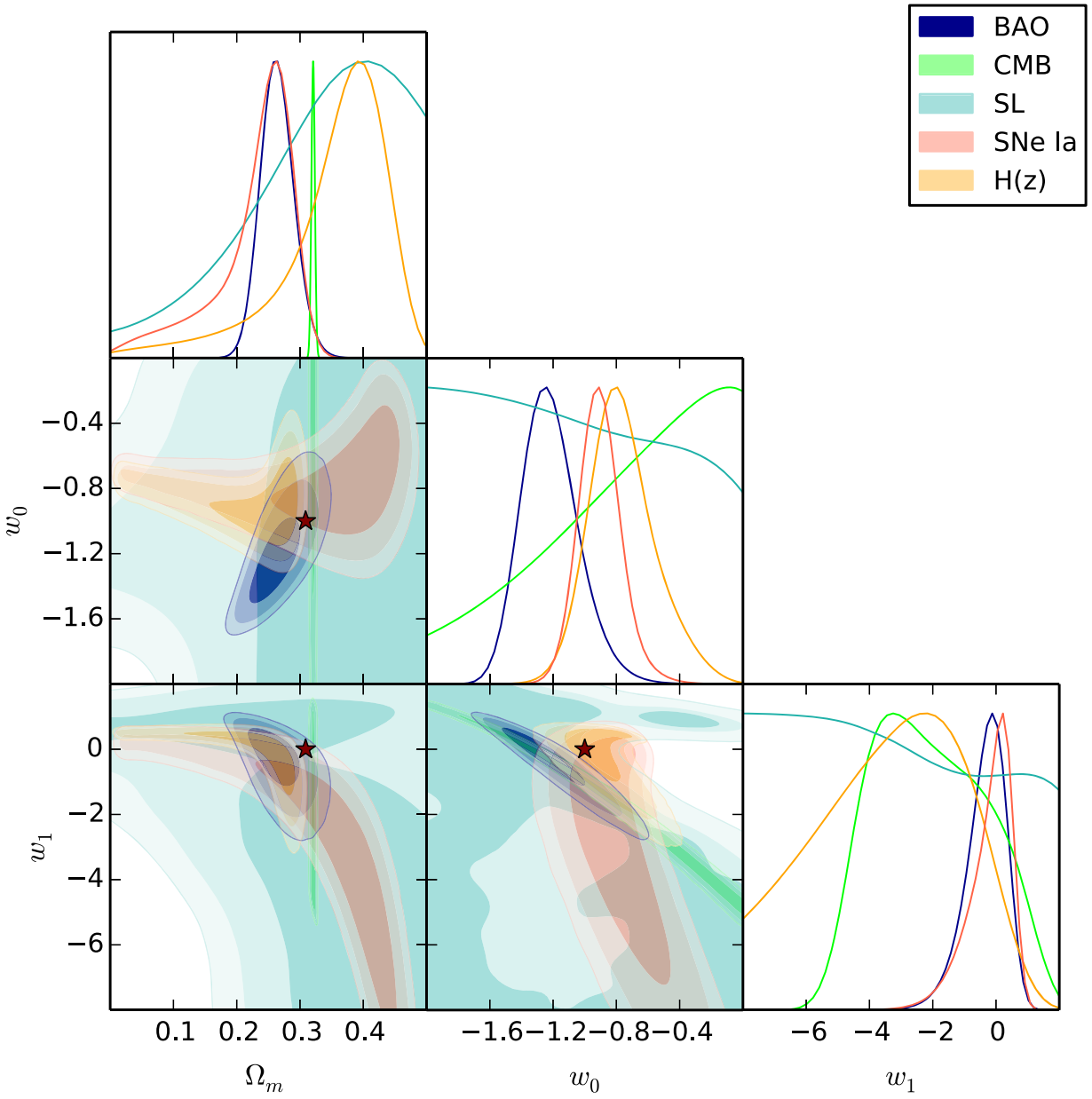

Figure 6. Same as Figure 4, but for the BA parameterization.

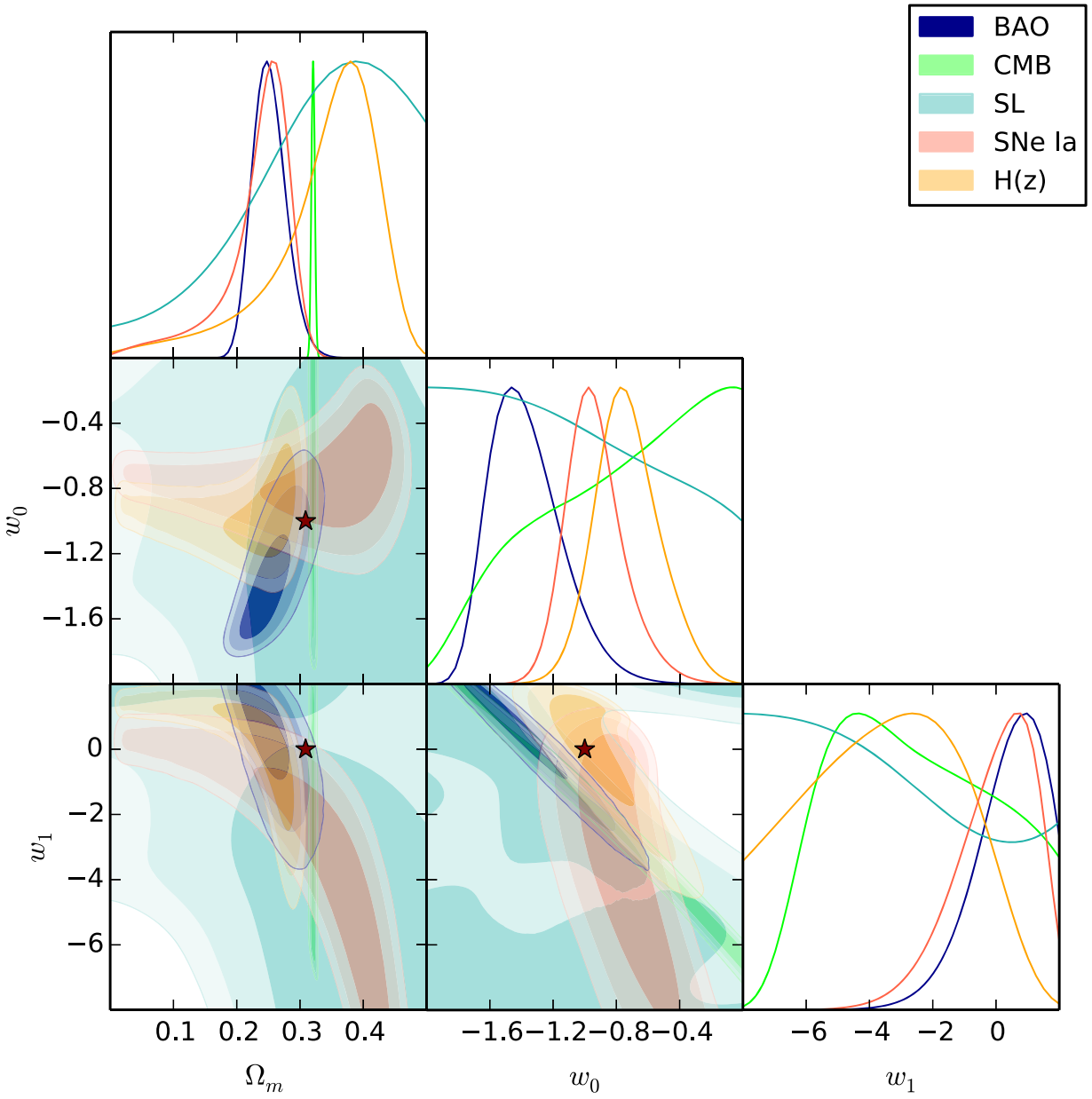

Figure 7. Same as Figure 4, but for the FSLL I parameterization.

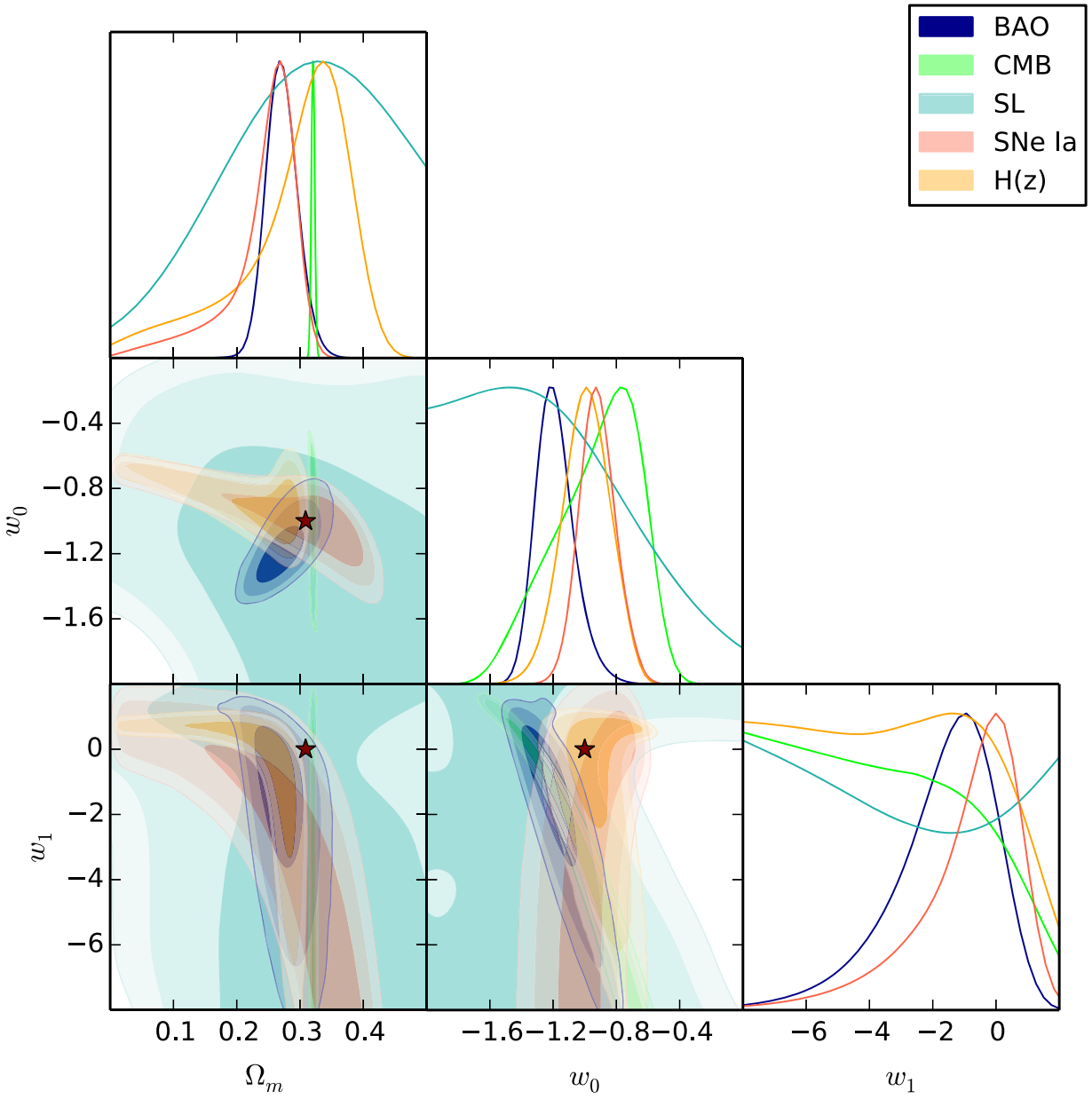

Figure 8. Same as Figure 4, but for the FSLL II parameterization.

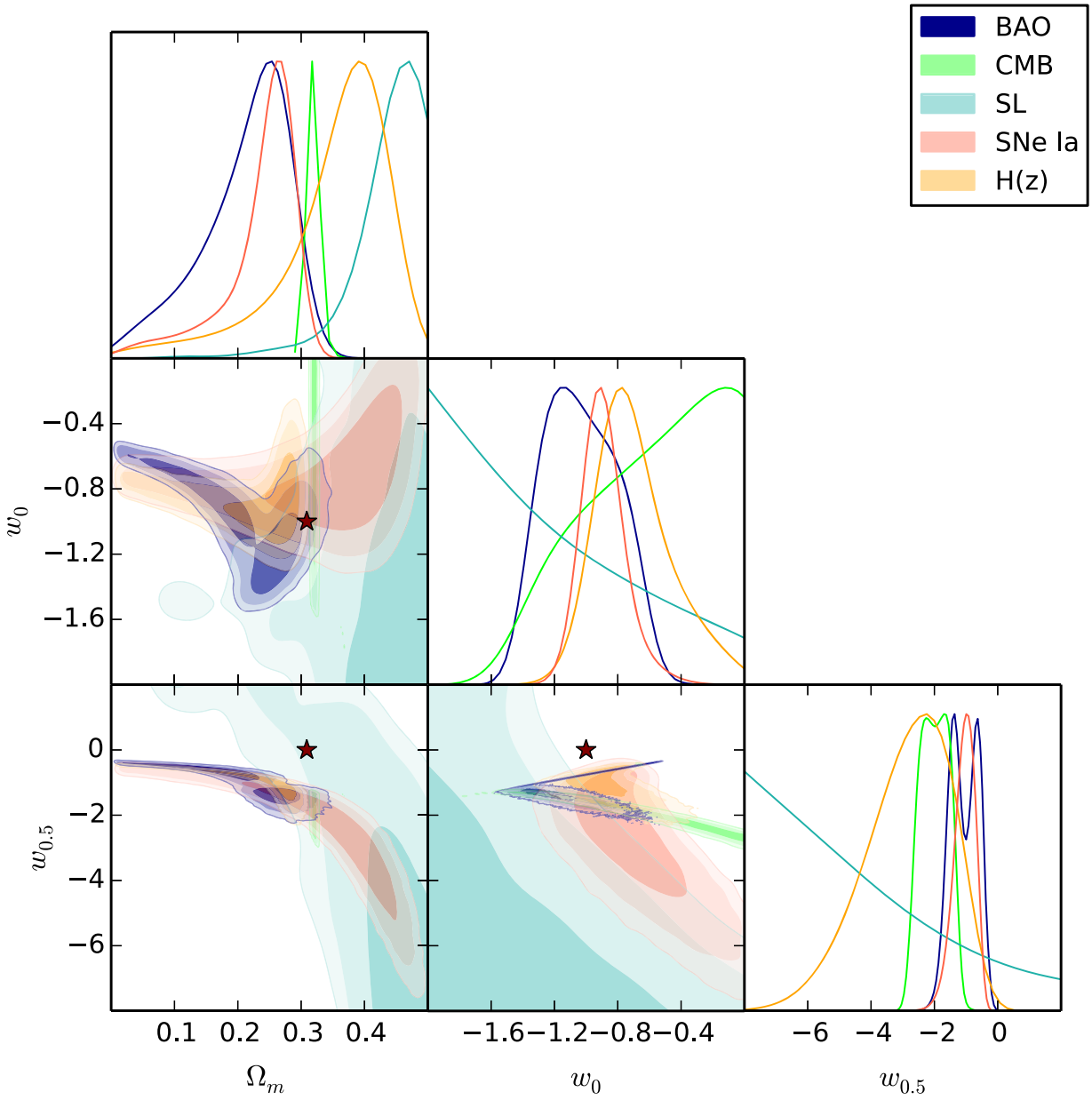

Figure 9. Same as Figure 4, but for the SeLa parameterization.

ORCID iDs

Ana Acebrón https://orcid.org/0000-0003-3108-9039
Verónica Motta https://orcid.org/0000-0003-4446-7465
Tomás Verdugo https://orcid.org/0000-0003-4062-6123
Eric Jullo https://orcid.org/0000-0002-9253-053X

References

Acebron, A., Jullo, E., Limousin, M., et al. 2017, MNRAS, 470, 1809
Albrecht, A., Bernstein, G., Cahn, R., et al. 2006, arXiv:astro-ph/0609591
Barboza, E. M., & Alcaniz, J. S. 2008, PhLB, 666, 415
Bayliss, M. B., Johnson, T., Gladders, M. D., Sharon, K., & Oguri, M. 2014, ApJ, 783, 41
Bina, D., Pelló, R., Richard, J., et al. 2016, A&A, 590, A14
Bond, J. R., Efstathiou, G., & Tegmark, M. 1997, MNRAS, 291, L33
Caminha, G. B., Grillo, C., Rosati, P., et al. 2016, A&A, 587, A80
Chevallier, M., & Polarski, D. 2001, IJMPD, 10, 213
Chirivì, G., Suyu, S. H., Grillo, C., et al. 2018, A&A, 614, A8
Copeland, E. J., Sami, M., & Tsujikawa, S. 2006, IJMPD, 15, 1753
D'Aloisio, A., & Natarajan, P. 2011, MNRAS, 411, 1628
Davis, T. M. 2014, GReGr, 46, 1731
Diego, J. M., Broadhurst, T., Benitez, N., et al. 2015, MNRAS, 446, 683
Eisenstein, D. J., & Hu, W. 1998, ApJ, 496, 605
Elíasdóttir, Á, Limousin, M., Richard, J., et al. 2007, arXiv:0710.5636
Feng, C.-J., Shen, X.-Y., Li, P., & Li, X.-Z. 2012, JCAP, 9, 023
Ferreira, E. G. M., Quintin, J., Costa, A. A., Abdalla, E., & Wang, B. 2017, PhRvD, 95, 043520
Foreman-Mackey, D., Hogg, D. W., Lang, D., & Goodman, J. 2013, PASP, 125, 306
Ganeshalingam, M., Li, W., & Filippenko, A. V. 2013, MNRAS, 433, 2240
Gaztanaga, E., Cabre, A., & Hui, L. 2009, MNRAS, 399, 1663
Giocoli, C., Bonamigo, M., Limousin, M., et al. 2016, MNRAS, 462, 167
Giocoli, C., Meneghetti, M., Bartelmann, M., Moscardini, L., & Boldrin, M. 2012, MNRAS, 421, 3343
Golse, G., Kneib, J.-P., & Soucail, G. 2002, A&A, 387, 788
Grillo, C., Suyu, S. H., Rosati, P., et al. 2015, ApJ, 800, 38
Harvey, D., Kneib, J. P., & Jauzac, M. 2016, MNRAS, 458, 660
Host, O. 2012, MNRAS, 420, L18
Hu, W., & Sugiyama, N. 1996, ApJ, 471, 542
Jaroszynski, M., & Kostrzewa-Rutkowska, Z. 2014, MNRAS, 439, 2432
Jassal, H. K., Bagla, J. S., & Padmanabhan, T. 2005a, PhRvD, 72, 103503

Jassal, H. K., Bagla, J. S., & Padmanabhan, T. 2005b, MNRAS, 356, L11
Jauzac, M., Clément, B., Limousin, M., et al. 2014, MNRAS, 443, 1549
Jimenez, R., & Loeb, A. 2002, ApJ, 573, 37
Joyce, A., Lombriser, L., & Schmidt, F. 2016, ARNPS, 66, 95
Jullo, E., Kneib, J.-P., Limousin, M., et al. 2007, NJPh, 9, 447
Jullo, E., Natarajan, P., Kneib, J.-P., et al. 2010, Sci, 329, 924
Kassiola, A., & Kovner, I. 1993, ApJ, 417, 450
Kneib, J.-P., Ellis, R. S., Smail, I., Couch, W. J., & Sharples, R. M. 1996, ApJ, 471, 643
Komatsu, E., et al. 2011, ApJS, 192, 18
Lazkoz, R., Nesseris, S., & Perivolaropoulos, L. 2005, JCAP, 11, 010
Li, M., Li, X.-D., Wang, S., & Wang, Y. 2011, CoTPh, 56, 525
Limousin, M., Jullo, E., Richard, J., et al. 2010, A&A, 524, A95
Limousin, M., Kneib, J.-P., & Natarajan, P. 2005, MNRAS, 356, 309
Limousin, M., Morandi, A., Sereno, M., et al. 2013, SSRv, 177, 155
Limousin, M., Richard, J., Jullo, E., et al. 2007, ApJ, 668, 643
Limousin, M., Richard, J., Jullo, E., et al. 2016, A&A, 588, A99
Linder, E. V. 2003, PhRvL, 90, 091301
Link, R., & Pierce, M. J. 1998, ApJ, 502, 63
Magaña, J., Cárdenas, V. H., & Motta, V. 2014, JCAP, 1410, 017
Magaña, J., Motta, V., Cárdenas, V. H., & Foëx, G. 2017, MNRAS, 469, 47
Magaña, J., Motta, V., Cardenas, V. H., Verdugo, T., & Jullo, E. 2015, ApJ, 813, 69
McCully, C., Keeton, C. R., Wong, K. C., & Zabludoff, A. I. 2014, MNRAS, 443, 3631
McCully, C., Keeton, C. R., Wong, K. C., & Zabludoff, A. I. 2017, ApJ, 836, 141
Meneghetti, M., Natarajan, P., Coe, D., et al. 2017, MNRAS, 472, 3177
Miralda-Escude, J., & Babul, A. 1995, ApJ, 449, 18
Monna, A., Seitz, S., Balestra, I., et al. 2017, MNRAS, 466, 4094
Mortonson, M. J., Weinberg, D. H., & White, M. 2014, arXiv:1401.0046
Neveu, J., Ruhlmann-Kleider, V., Astier, P., et al. 2017, A&A, 600, A40
Pantazis, G., Nesseris, S., & Perivolaropoulos, L. 2016, PhRvD, 93, 103503
Perlmutter, S., Aldering, G., Goldhaber, G., et al. 1999, ApJ, 517, 565
Planck Collaboration, Ade, P. A. R., Aghanim, N., et al. 2016a, A&A, 594, A13
Planck Collaboration, Ade, P. A. R., Aghanim, N., et al. 2016b, A&A, 594, A14
Riess, A. G., Filippenko, A. V., Challis, P., et al. 1998, AJ, 116, 1009
Salvatelli, V., Said, N., Bruni, M., Melchiorri, A., & Wands, D. 2014, PhRvL, 113, 181301
Sendra, I., & Lazkoz, R. 2012, MNRAS, 422, 776
Soucail, G., Kneib, J.-P., & Golse, G. 2004, A&A, 417, L33
Tu, H., Limousin, M., Fort, B., et al. 2008, MNRAS, 386, 1169
Umetsu, K., Sereno, M., Medezinski, E., et al. 2015, ApJ, 806, 207
Wang, L., Li, C., Kauffmann, G., & De Lucia, G. 2006, MNRAS, 371, 537
Wang, S., Hu, Y., Li, M., & Li, N. 2016, ApJ, 821, 60
Wang, Y. 2008, PhRvD, 77, 123525
Wang, Y., Chuang, C.-H., & Mukherjee, P. 2012, PhRvD, 85, 023517
Weinberg, S. 1989, RvMP, 61, 1
Zeldovich, Y. B. 1968, SvPhU, 11, 381
Zhao, G.-B., Raveri, M., Pogosian, L., et al. 2017, NatAs, 1, 627
Zitrin, A., Fabris, A., Merten, J., et al. 2015, ApJ, 801, 44
Zitrin, A., Rosati, P., Nonino, M., et al. 2012, ApJ, 749, 97